Virgo calibration and reconstruction of the gravitationnal wave strain during VSR1

To cite this article: T Accadia *et al* 2010 *J. Phys.: Conf. Ser.* **228** 012015

View the article online for updates and enhancements.

Virgo calibration and reconstruction of the gravitationnal wave strain during VSR1

T. Accadia[12], F. Acernese[6ac], F. Antonucci[9a], S. Aoudia[15a],
K. G. Arun[11], P. Astone[9a], G. Ballardin[2], F. Barone[6ac],
M. Barsuglia[1], Th. S. Bauer[14a], M.G. Beker[14a], A. Belletoile[12],
S. Bigotta[8ab], S. Birindelli[15a], M. Bitossi[8a], M. A. Bizouard[11],
M. Blom[14a], C. Boccara[3], F. Bondu[15b], L. Bonelli[8ab], R. Bonnand[13],
L. Bosi[7a], S. Braccini[8a], C. Bradaschia[8a], A. Brillet[15a], V. Brisson[11],
R. Budziński[17b], T. Bulik[17cd], H. J. Bulten[14ab], D. Buskulic[12],
C. Buy[1], G. Cagnoli[4a], E. Calloni[6ab], E. Campagna[4ab], B. Canuel[2],
F. Carbognani[2], F. Cavalier[11], R. Cavalieri[2], G. Cella[8a], E. Cesarini[4b],
E. Chassande-Mottin[1], A. Chincarini[5], F. Cleva[15a], E. Coccia[10ab],
C. N. Colacino[8a], J. Colas[2], A. Colla[9ab], M. Colombini[9b], A. Corsi[9a],
J.-P. Coulon[15a], E. Cuoco[2], S. D'Antonio[10a], A. Dari[7ab], V. Dattilo[2],
M. Davier[11], R. Day[2], R. De Rosa[6ab], M. del Prete[8ac], L. Di Fiore[6a],
A. Di Lieto[8ab], M. Di Paolo Emilio[10ac], A. Di Virgilio[8a], A. Dietz[12],
M. Drago[16cd], V. Fafone[10ab], I. Ferrante[8ab], F. Fidecaro[8ab], I. Fiori[2],
R. Flaminio[13], J.-D. Fournier[15a], J. Franc[13], S. Frasca[9ab],
F. Frasconi[8a], A. Freise[*], M. Galimberti[13], L. Gammaitoni[7ab],
F. Garufi[6ab], G. Gemme[5], E. Genin[2], A. Gennai[8a], A. Giazotto[8a],
R. Gouaty[12], M. Granata[1], C. Greverie[15a], G. M. Guidi[4ab],
H. Heitmann[15], P. Hello[11], S. Hild[**], D. Huet[2], P. Jaranowski[17e],
I. Kowalska[17c], A. Królak[17af], N. Leroy[11], N. Letendre[12],
T. G. F. Li[14a], M. Lorenzini[4a], V. Loriette[3], G. Losurdo[4a],
J. M. Mackowski[13], E. Majorana[9a], I. Maksimovic[3], N. Man[15a],
M. Mantovani[8ac], F. Marchesoni[7a], F. Marion[12], J. Marque[2],
F. Martelli[4ab], A. Masserot[12], C. Michel[13], L. Milano[6ab],
Y. Minenkov[10a], M. Mohan[2], J. Moreau[3], N. Morgado[13],
A. Morgia[10ab], S. Mosca[6ab], V. Moscatelli[9a], B. Mours[12], I. Neri[7ab],
F. Nocera[2], G. Pagliaroli[10ac], L. Palladino[10ac], C. Palomba[9a],
F. Paoletti[8a,2], S. Pardi[6ab], M. Parisi[6b], A. Pasqualetti[2],
R. Passaquieti[8ab], D. Passuello[8a], G. Persichetti[6ab], M. Pichot[15a],
F. Piergiovanni[4ab], M. Pietka[17e], L. Pinard[13], R. Poggiani[8ab],
M. Prato[5], G. A. Prodi[16ab], M. Punturo[7a], P. Puppo[9a], O. Rabaste[1],
D. S. Rabeling[14ab], P. Rapagnani[9ab], V. Re[16ab], T. Regimbau[15a],
F. Ricci[9ab], F. Robinet[11], A. Rocchi[10a], L. Rolland[12], R. Romano[6ac],
D. Rosińska[17g], P. Ruggi[2], B. Sassolas[13], D. Sentenac[2], R. Sturani[4ab],
B. Swinkels[2], A. Toncelli[8ab], M. Tonelli[8ab], O. Torre[8ac],
E. Tournefier[12], F. Travasso[7ab], J. Trummer[12], G. Vajente[8ab],
J. F. J. van den Brand[14ab], S. van der Putten[14a], M. Vavoulidis[11],
G. Vedovato[16c], D. Verkindt[12], F. Vetrano[4ab], A. Viceré[4ab],

J.-Y. Vinet[15a], H. Vocca[7a], M. Was[11], M. Yvert[12]

[1]AstroParticule et Cosmologie (APC), CNRS: UMR7164-IN2P3-Observatoire de Paris-Université Denis Diderot-Paris 7 - CEA : DSM/IRFU

[2]European Gravitational Observatory (EGO), I-56021 Cascina (Pi), Italy

[3]ESPCI, CNRS, F-75005 Paris, France

[4]INFN, Sezione di Firenze, I-50019 Sesto Fiorentino[a]; Università degli Studi di Urbino 'Carlo Bo', I-61029 Urbino[b], Italy

[5]INFN, Sezione di Genova; I-16146 Genova, Italy

[6]INFN, sezione di Napoli [a]; Università di Napoli 'Federico II'[b] Complesso Universitario di Monte S.Angelo, I-80126 Napoli; Università di Salerno, Fisciano, I-84084 Salerno[c], Italy

[7]INFN, Sezione di Perugia[a]; Università di Perugia[b], I-6123 Perugia,Italy

[8]INFN, Sezione di Pisa[a]; Università di Pisa[b]; I-56127 Pisa; Università di Siena, I-53100 Siena[c], Italy

[9]INFN, Sezione di Roma[a]; Università 'La Sapienza'[b], I-00185 Roma, Italy

[10]INFN, Sezione di Roma Tor Vergata[a]; Università di Roma Tor Vergata[b]; Università dell'Aquila, I-67100 L'Aquila[c], Italy

[11]LAL, Université Paris-Sud, IN2P3/CNRS, F-91898 Orsay, France

[12]Laboratoire d'Annecy-le-Vieux de Physique des Particules (LAPP), IN2P3/CNRS, Université de Savoie, F-74941 Annecy-le-Vieux, France

[13]Laboratoire des Matériaux Avancés (LMA), IN2P3/CNRS, F-69622 Villeurbanne, Lyon, France

[14]Nikhef, National Institute for Subatomic Physics, P.O. Box 41882, 1009 DB Amsterdam[a]; VU University Amsterdam, De Boelelaan 1081, 1081 HV Amsterdam[b], The Netherlands

[15]Université Nice-Sophia-Antipolis, CNRS, Observatoire de la Côte d'Azur, F-06304 Nice[a]; Institut de Physique de Rennes, CNRS, Université de Rennes 1, 35042 Rennes[b]; France

[16]INFN, Gruppo Collegato di Trento[a] and Università di Trento[b], I-38050 Povo, Trento, Italy; INFN, Sezione di Padova[c] and Università di Padova[d], I-35131 Padova, Italy

[17]IM-PAN 00-956 Warsaw[a]; Warsaw Univ. 00-681 Warsaw[b]; Astro. Obs. Warsaw Univ. 00-478 Warsaw[c]; CAMK-PAN 00-716 Warsaw[d]; Białystok Univ. 15-424 Bial ystok[e]; IPJ 05-400 Świerk-Otwock[f]; Inst. of Astronomy 65-265 Zielona Góra[g], Poland

[*]University of Birmingham, Birmingham, B15 2TT, United Kingdom

[**]University of Glasgow, Glasgow, G12 8QQ, United Kingdom

E-mail: `rollandl@in2p3.fr`

Abstract. Virgo is a kilometer-length interferometer for gravitationnal waves detection located near Pisa. Its first science run, VSR1, occured from May to October 2007. The aims of the calibration are to measure the detector sensitivity and to reconstruct the time series of the gravitationnal wave strain $h(t)$.

The absolute length calibration is based on an original non-linear reconstruction of the differential arm length variations in free swinging Michelson configurations. It uses the laser wavelength as length standard. This method is used to calibrate the frequency dependent response of the Virgo mirror actuators and derive the detector in-loop response and sensitivity within $\sim 5\%$.

The principle of the strain reconstruction is highlighted and the $h(t)$ systematic errors are estimated. A photon calibrator is used to check the sign of $h(t)$. The reconstructed $h(t)$ during VSR1 is valid from 10 Hz up to 10 kHz with systematic errors estimated to 6% in amplitude. The phase error is estimated to be 70 mrad below 1.9 kHz and $6\,\mu$s above.

1. Introduction

The Virgo detector [1] is a kilometer-length interferometer (ITF) located near Pisa (Italy). It is designed to search for gravitational waves (GW) in the frequency range from 10 Hz to a few kHz. Expected astrophysical sources of detectable GWs are compact objects such as neutrons stars or black holes.

The Virgo first science run (VSR1) was performed from May 18th to October 1st 2007 with a sensitivity close to its nominal one, and in coincidence to the end of the fifth science run (S5) of the three LIGO detectors [2]. In order to reduce the false detection rate and improve the estimation of the parameters of potential sources, the data of all the detectors are used together to search for a GW signal.

The purpose of the Virgo calibration is to measure the parameters needed (i) to estimate the ITF sensitivity to GW strain as a function of frequency, $\tilde{h}(f)$, and (ii) to reconstruct from the ITF data the amplitude $h(t)$ of the GW strain signal. To achieve optimum sensitivity, the positions of the different mirrors are controlled [3] to have, in particular, beam resonance in the cavities, destructive interference at the ITF output port and to compensate for environmental noise. The controls would also attenuate the effect of a passing GW below a few hundreds hertz. A synopsis of the longitudinal control loop and its components is given in figure 1. The effects of the longitudinal controls have thus to be precisely calibrated in the frequency domain. Above a few hundreds hertz, the mirrors behave as free falling masses in the longitudinal direction. The main effect of a passing GW would then be a frequency-dependent variation of the power at the ITF output. characterized by the ITF optical response. Finally, the readout electronics of the output power and its timing precision have also to be calibrated.

In this paper, the main method used to get an absolute length calibration is first described and the mirror actuator calibration results are highlighted. The way the Virgo sensitivity is measured is then shown. In the last section, the principle of the h(t) reconstruction is described as well as some measurements performed to estimate the errors on the h(t) signal.

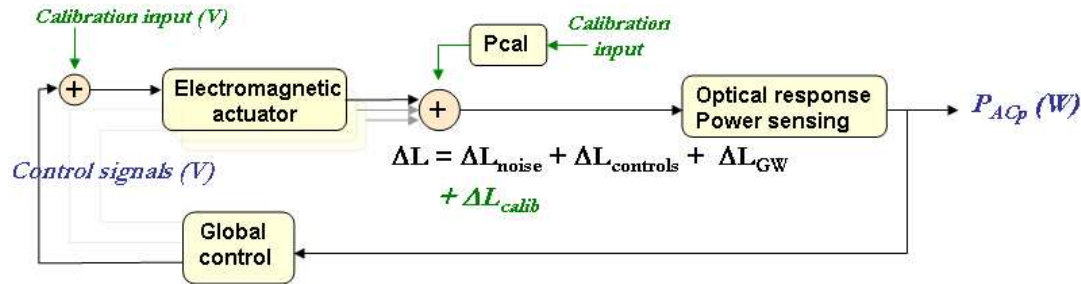**Figure 1.** Synopsis of the Virgo longitudinal control loop. A variation of the differential length of the arms of the ITF, ΔL, is sensed through the optical response which converts the length variation into laser power variation at the ITF output port. The power impinging on photodiodes is read and sampled at 20 kHz in the channel P_{ACp} (W). This channel is used as error signal to compute the control signals (V) sent to the different mirror actuators.
Calibration signals can be injected into the loop to force differential length variations ΔL_{calib}. The standard path is through the electromagnetic actuators. An auxiliary setup, the photon calibrator (pcal), can also be used (see section 4.3).

2. Absolute length measurement for mirror actuation calibration

The ITF calibration is based on absolute length measurements. The displacement induced by the mirror actuators is reconstructed using the ITF as a simple Michelson. The non-linear method used to reconstruct the arm differential motion in the freely swinging Michelson with passing fringes is described. The laser wavelength is used as length standard.

Mirrors of the Virgo ITF are mis-aligned to get a simple Michelson configuration. Different configurations are used to calibrate the beam-splitter and arm mirrors actuations (comprising the beam-splitter, one end mirror and the input mirror in the other arm). The typical results of the mirror actuation calibration are given.

2.1. Absolute length measurement

In a simple Michelson ITF, the phase difference $\Delta\Phi$ between the two interfering beams is function of the differential arm length ΔL, using the laser wavelength $\lambda = 1064\,$nm as standard: $\Delta\Phi(t) = \frac{4\pi}{\lambda}\Delta L(t)$.

In a simple Michelson ITF with frontal phase-modulation, the power of the output beam ($\mathcal{P}_{DC}$) as well as the demodulated power ($\mathcal{P}_{AC}$) signals are functions of the phase difference $\Delta\Phi$ between the two interfering beams: $\mathcal{P}_{DC} = \beta(1 - \gamma\cos(\Delta\Phi))$ and $\mathcal{P}_{AC} = \alpha\sin(\Delta\Phi)$, where α and β are proportional to the laser power and γ is proportional to the ITF contrast. Therefore, in the $(\mathcal{P}_{DC}, \mathcal{P}_{AC})$ plane, the signal follows an ellipse as shown in figure 2.

The measurement of the differential arm length ΔL requires a non-linear reconstruction. The ellipse is fitted using the method described in [4]. The fit gives the ellipse center position (theoretically $(\beta,0)$) and the axis widths (theoretically $(\beta\gamma,\alpha)$). The variations of the parameters α, β and γ are monitored and found to be of the order of 0.5% during a few-minute dataset. $\Delta\Phi'$ can then be estimated directly from the ITF signals as the angle between the ellipse axis along DC and the line from the ellipse center to the current point position $(\mathcal{P}_{DC}, \mathcal{P}_{AC})$. Using a suitable ellipse tour counting, the right number of 2π is added to $\Delta\Phi'$ to recover completely the angle $\Delta\Phi$. The differential arm length ΔL_{rec} is then computed from equation 2.1.

Figure 3 is an illustration of the method. In the window Δt, 6 interfringes passed on the DC signal: It indicates a differential arm elongation of $6 \times \frac{\lambda}{2} = 3.19\,\mu$m. In the same window, the reconstructed ΔL varies by $\sim 3.18\,\mu$m.
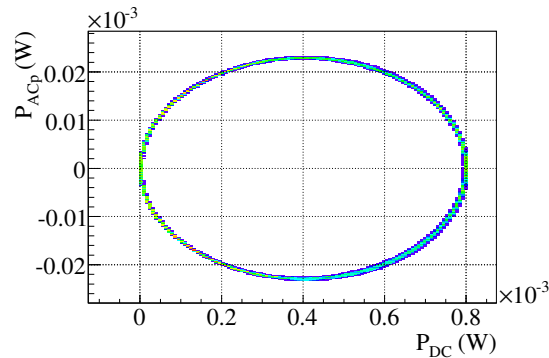

Figure 2. $\mathcal{P}_{AC}$ vs $\mathcal{P}_{DC}$ measured in free swinging Michelson data (configuration comprising the beam-splitter and the two arm input mirrors).
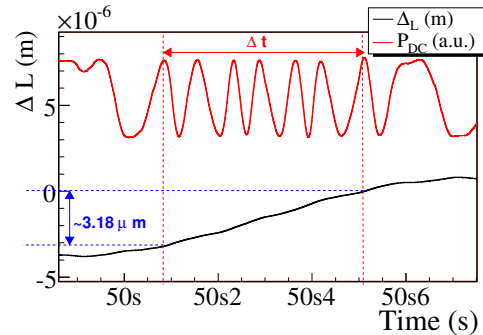
Figure 3. Red curve (top): measured time series of $\mathcal{P}_{DC}$ in free swinging Michelson data, in arbitrary units. Black curve (bottom): reconstructed time series of ΔL, in meters.

2.2. Mirror actuator calibration

The Virgo electromagnetic actuators are used to induce a longitudinal motion to the suspended mirrors from a voltage signal. As shown in figure 4, the signals pass through some electronics and pairs of coil-magnet (A) and the pendulum mechanical response (P). Their calibration consists in measuring the transfer function between the input voltage V_{inj} and the induced motion ΔL_{inj}. This is done setting the ITF in free swinging Michelson configurations: sine signals V_{inj} are injected to the actuators and the motion ΔL_{rec} is rescontructed using the method described in section 2.1. The complete response of the ITF is shown in figure 4: the reconstructed ΔL_{rec} has to be corrected for some effects to get the true induced mirror motion ΔL_{inj}, mainly some delays due to the light propagation time in the arms (O) and due to the output power readout electronics (S).

Thirteen sine signals have been injected from 5 Hz to 1. kHz. Such injections were done at different amplitudes in order to check the linearity of the measurements. They were also performed every two weeks during VSR1 in order to monitor their time stability. The mirror actuation responses $\Delta L_{inj}/V_{inj}$ are measured with a statistical error better than 1%. A regular monitoring of the actuation has shown $\sim 2\%$ variations and different measurements had up to $\sim 2\%$ offsets from the standard measurements. Systematic errors of the order of 4% on the modulus and 50 mrad on the phase have been derived.
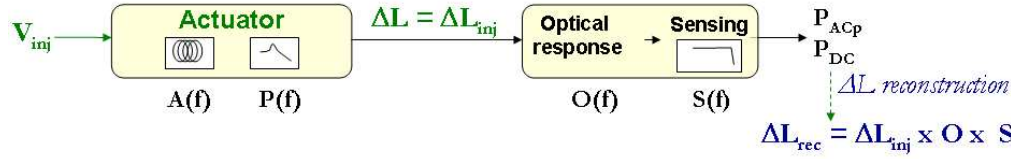

Figure 4. Signal processing in the free swinging Michelson data used for the mirror actuation calibration. See text for details.

3. Virgo ITF response and sensitivity measurements

The first goal of the calibration is to measure the Virgo sensitivity. It is based on the knowledge of a mirror actuator response calibrated as shown in section 2. The ITF response in closed-loop is first measured and then used to estimated the ITF sensitivity.

3.1. Virgo ITF response

The ITF response, in W/m, is the the transfer function from the differential arm length variation ΔL to the ITF output power $\mathcal{P}_{ACp}$. When the Virgo ITF is in closed-loop (see figure 1), some white noise V_{inj} is injected up to 1.5 kHz through an end mirror actuator. Using the actuator calibration, the induced ΔL_{inj} is derived. The transfer function $\Delta L_{inj}/\mathcal{P}_{ACp}$ (inverse of the ITF response) is then measured up to ~ 1.5 kHz.

The longitudinal controls do not act above a few hundred Hz: the ITF response is only the optical response and the output power sensing. A simple model is thus fit to the measured transfer function from 800 Hz to 1 kHz. The optical response is modeled by a simple pole at 500 Hz due to the arm cavities with finesse 50. The finesse of the arm cavities changes over time by as much as 3%. These variations are ignored at this stage. The gain of the optical response is let free in the fit. The measurements of the output power sensing are not described in this paper: the fitted model of the sensing lies within 2% in modulus and 20 mrad in phase from the measured response up to 6 kHz.

An example of a measured inverse ITF response during VSR1 is given in figure 5.

3.2. Virgo sensitivity

The Virgo sensitivity is measured from the ITF response in closed-loop, in m/W, and from the spectrum of the output signal $\mathcal{P}_{ACp}$, in W: they are multiplied to get the sensitivity in meters. It is then divided by the Virgo arm length, 3 km, to get the sensitivity in strain as shown in figure 6. The sensitivity is measured a few minutes after the ITF response in order to avoid possible variations of the optical gain.

Note that the sensitivity is measured with systematic errors of the order of 4% coming from the mirror actuator calibration below 1 kHz. The errors above 1 kHz are higher (5–10%) due to (i) the use of a fixed cavity finesse, (ii) the power sensing model errors and (iii) the fact that the controls were not totally negligible in the fitted frequency range during VSR1.
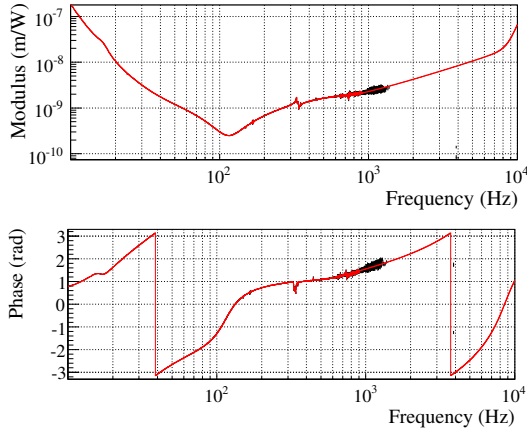
Figure 5. Virgo ITF response measured in September 2007. Black: measured transfer function up to 1.5 kHz (with increasing statistical uncertainties above a few 100's Hz). Red: extrapolated transfer function.
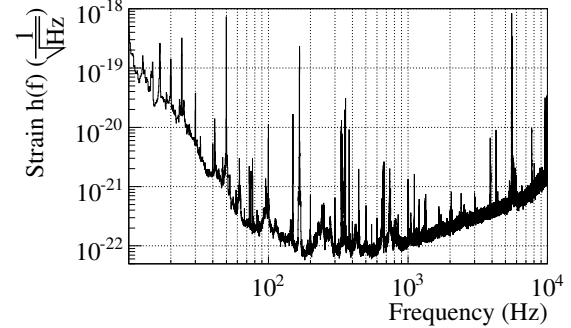

Figure 6. Virgo sensitivity measured in September 2007.

4. h(t) strain reconstruction

The second aim of the calibration process is the reconstruction of the GW strain time series $h(t)$. The principle of the reconstruction used for the VSR1 data is described. Some estimations of the errors and the sign of $h(t)$ are then given.

4.1. Reconstruction principle

The principle of the reconstruction of $h(t)$ from the ITF output power and the mirror longitudinal controls is given in figure 7. The effective arm differential length variation $\Delta L_{effective}$ is reconstructed in the frequency domain from the output power $\mathcal{P}_{ACp}$ and the calibrated optical response and power sensing. It contains the contribution from the noise, from the controls and possibly from the GWs. The contributions from the controls are reconstructed in the frequency domain from the correction signals sent to the mirror actuators knowing the actuator responses. They are then subtracted from $\Delta L_{effective}$ to get the final ΔL with the noise and GW contributions only. The result is then divided by 3 km and put back in the time domain to get the strain $h(t)$. The contribution from the power line (50 Hz and harmonics) is finally subtracted.

4.2. Error estimation using mirror actuators

In order to estimate the errors on the reconstructed strain $h(t)$, some datasets with sine signals V_{inj} injected to an out-of-loop mirror (an input mirror) were taken every week during VSR1. It corresponds to an injected strain $h_{inj} = \Delta L_{inj}/(3000\,\text{m})$. The transfer function of the reconstructed over injected strain h/h_{inj} is then measured. This transfer function is expected to be flat: at 0 in phase and at 0.97 in modulus (since the motion of the input mirror changes both the arm length and the Michelson length, the optical response of Virgo is 3% lower for an input mirror than for an end mirror).

The differential arm length variations ΔL_{inj} induced by the injected signal is derived from the mirror actuation calibration, with errors of the order of 4% in modulus and 50 mrad in phase.

The transfer function measured every week during VSR1 is shown in figure 8. The observed
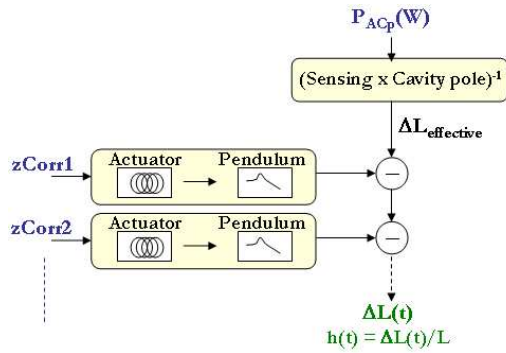
Figure 7. Synopsis of the reconstruction of $h(t)$ from the ITF output power $\mathcal{P}_{ACp}$ and the longitudinal correction signals sent to the mirror actuators ($zCorr$ channels). See text for details.
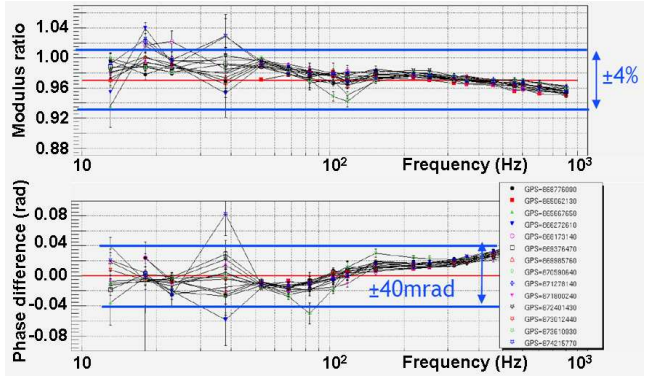

Figure 8. Top curve: ratio between the reconstructed amplitude of the lines in $h(t)$ and the expected injected amplitude. Bottom curve: phase difference for the two signals. The difference symbols correspond to different measurements performed once per week during VSR1.

time variations at a given frequency are compatible with statistical errors. The difference between the measurements and the expected values gives an estimation of the systematic errors on the reconstructed strain $h(t)$. They are of the order of 4% in modulus and 50 mrad in phase below 1 kHz. This is compatible with the estimated systematic errors of the mirror actuation calibration used in the $h(t)$ reconstruction.

4.3. "Photon calibrator" and sign of $h(t)$
As in GEO [5] and LIGO [6, 7], a photon calibrator (pcal) was setup in Virgo during VSR1. It is used as an independent mirror actuator: the radiation pressure of an auxiliary laser is used to displace one input mirror. Its main use during VSR1 has been to check the sign of $h(t)$, defined in common with LIGO as $h = \frac{L_x - L_y}{L}$ where, in Virgo, x and y are the north and west arms respectively.

Sine signals injections were performed with the Virgo pcal, corresponding to an expected signal h_{inj}. The phase between the reconstructed h and the expected one h_{inj} has been measured below 1 kHz. It is expected to be 0. The phase at low frequency converges to 0 within 15 mrad: this proves that the sign of the reconstructed $h(t)$ is correct.

Note that the pcal has been used also to cross-check the mirror actuation standard calibration. It agrees within the large pcal systematic errors of 20%.

5. Conclusion
The Virgo standard calibration is based on a non-linear reconstruction of the error signal in free swinging Michelson configurations. It relies on the laser wavelength as length standard. It has been used to calibrate the mirror electromagnetic actuators within 4% in modulus and 50 mrad in phase.

The Virgo photon calibrator has been mainly used to check the sign of $h(t)$.

The principle of the reconstruction of the strain $h(t)$ applied on the VSR1 data has been given along with some estimations of the errors. Some other sources of errors must be taken into account, especially from the ITF output power sensing and from some timing issues. Taking them into account, the reconstructed $h(t)$ during VSR1 is valid from 10 Hz up to the Nyquist

frequency of the channel (2048 Hz, 8192 Hz or 10000 Hz) with systematic errors estimated to 6% in amplitude. The phase error is estimated to be 70 mrad below 1.9 kHz and $6\,\mu$s above.

References

[1] The Virgo collaboration 1997 *Final Design Report* Virgo Technical Note VIR-TRE-DIR-1000-13
[2] Abbott B et al 2004 *Nuclear Instruments and Methods for Physics Research* **517** pp 154–179
[3] Acernese et al (Virgo collaboration) 2008 *Astroparticle Physics* **30** pp 29–38
[4] Halíř R and Flusser J 1998 *Proc. of the 6th International Conference in Central Europe on Computer Graphics, Visualisation and Interactive Digital Media. WSCG 98* (Bory, Czech Republic) pp 125–132
[5] Hild S et al 2007 *Class. Quantum Grav.* **24** pp 5681–5688
[6] Goetz E et al submitted to CQG
[7] Savage R *these proceedings*